Letter

Excitonic wave-packet evolution in a two-orbital Hubbard model chain: A real-time real-space study

Bradraj Pandey,[1,2] Gonzalo Alvarez,[3] and Elbio Dagotto[1,2]
[1]*Department of Physics and Astronomy, University of Tennessee, Knoxville, Tennessee 37996, USA*
[2]*Materials Science and Technology Division, Oak Ridge National Laboratory, Oak Ridge, Tennessee 37831, USA*
[3]*Computational Sciences and Engineering Division and Center for Nanophase Materials Sciences, Oak Ridge National Laboratory, Oak Ridge, Tennessee 37831, USA*

(Received 21 August 2021; revised 2 December 2021; accepted 6 December 2021; published 17 December 2021)

Motivated by experimental developments introducing the concept of spin-orbit separation, we study the real-space real-time evolution of an excitonic wave packet using a two-orbital Hubbard model in a chain. The exciton is created by exciting an electron from a lower-energy half-filled orbital to a higher-energy empty orbital. We carry out the real-time dynamics of the resulting excitonic wave packet using the time-dependent density matrix renormalization group. We find clear evidence of charge-spin and spin-orbit separation in real space, by tracking the time evolution of local observables. We show that the velocity of the orbiton can be tuned varying the interorbital interactions. We also present a comparative study of the dynamics of a hole in one-orbital and two-orbital Hubbard models. Moreover, we analyze the dynamics of an exciton with spin-flip excitation, where we observe fractionalized spinons induced by Hund's interaction.

DOI: 10.1103/PhysRevB.104.L220302

Introduction. The dynamics of excitations in low-dimensional compounds has attracted considerable attention [1,2]. Experimentally observed excitations include holons, spinons, doublons, and excitons [3,4]. In particular, the study of excitons in multiband insulators unveiled interesting surprises [5,6]. Localized and delocalized charge-transfer excitons were observed experimentally in La_2CuO_4 and La_2NiO_4, respectively [7]. More recently, spin-orbit excitons were observed in Sr_2IrO_4 using resonant inelastic x-ray scattering (RIXS) [8]. The excitonic dynamic in Sr_2IrO_4 was described as analogous to the propagation of holes in a cuprate's antiferromagnetic (AFM) background [9].

Due to reduced dimensionality and strong correlation effects, quasi-one-dimensional (quasi-1D) systems display exotic dynamical properties [10–12], including the fractionalization of low-energy excitations [1,3] into spin (spinons) and charge (holons) excitations propagating with different velocities [13–15]. The existence of spin-charge separation was shown experimentally early on in quasi-one-dimensional systems [16,17]. Interestingly, the fractionalization of electronic excitations is not limited to spin and charge; it can also include the orbital degree of freedom [18]. In fact, spin-orbital separation was observed experimentally in the transition metal compound Sr_2CuO_3 [19]. Using high-resolution RIXS experiments, spin-orbital separation was also observed in the ladder system $CaCu_2O_3$ [20].

Recently, the spin-orbit separation in Mott insulating systems was studied theoretically using the effective Kugel-Khomskii model [21]. In the limit of vanishing Hund's coupling, the propagation of the orbiton in a ferro-orbital and antiferromagnetic chain was shown to map into a "single hole" moving in an AFM chain with its dynamics described by an effective t-J model [21]. However, in transition metal compounds, the Hund's interaction plays an important role, and depending on the material, it can be strong. Precisely for a strong Hund's coupling, in the propagation of an orbiton, the interorbital ferromagnetic (FM) and AFM spin alignments (in the excited states of the superexchange process) are not equal, and the simple mapping between orbiton and t-J hole dynamics is no longer valid [22,23]. More recently, using RIXS, the effect of Hund's interaction on the orbiton propagation in a quasi-1D AFM compound Ca_2CuO_3 was studied [23]. It was observed that robust Hund's interactions are required in the theoretical description to understand the experimental orbital spectrum [23].

In this Research Letter, we provide a study of spin-orbit separation in a real-time and real-space formalism by creating a finite momentum excitonic wave packet at time $t = 0$, using a one-dimensional chain with two orbitals at each site. This wave packet is created by exciting an electron from a half-filled orbital to an empty higher-energy orbital, as in experiments. Previous studies primarily focused on the spectral properties to study spin-orbit separation and for simplicity relied on Kugel-Khomskii models in the strong-coupling limit [21,22,24]. Here, we consider a more general multiorbital Hubbard Hamiltonian at intermediate coupling strengths, accounting also for charge fluctuations and with focus on the influence of the Hund's coupling. To study the excitonic real-time dynamics, we use the time-dependent density-matrix renormalization group (t-DMRG) method [25,26]. We have observed that after creating the exciton, the hole (in the half-filled orbital) and the electron (in the empty orbital) always move together, while the spin wave packet in the half-filled orbital independently evolves from the charge wave packet. We also compare the dynamics of a hole in a one-orbital chain versus the dynamics of a hole in a two-orbital chain. Overall, at intermediate coupling and for robust values of the Hund's interaction, we find clear evidence of spin-orbit

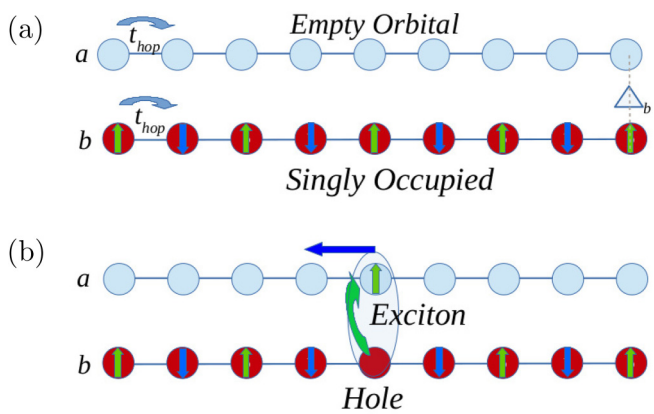

FIG. 1. Schematic representation of a one-dimensional chain with two orbitals (a and b) at each site. The blue circles represent orbital a, and the red circles represent orbital b. (a) The orbitals are separated by a large crystal field Δ. Orbital b is half filled, whereas orbital a is empty. (b) At $t = 0$ an exciton is created by exciting an electron from the half-filled orbital b (i.e., one electron per site in a staggered spin pattern) to orbital a, which is empty. The exciton has a finite momentum k_0 indicated by the blue arrow.

separation as time grows. Moreover, we quantitatively study the relation between the Hund's coupling and the orbiton velocity, finding that this orbiton's velocity increases with an increase in the Hund's coupling magnitude, while the spinon's velocity remains unaffected. Furthermore, we also present the dynamics of a spin-flip exciton (the previous discussion was for a spin-preserving exciton), where we find fractionalized spinons, induced by the strong Hund's coupling.

Model and method. We use the two-orbital Hubbard model on a chain. The model can be written as the sum of kinetic and interaction energy terms $H = H_k + H_{\rm in}$ [27]. The kinetic (tight binding) portion contains the nearest-neighbor hopping along the chain direction defined as

$$H_k = -t_{\rm hop} \sum_{\langle ij\rangle,\sigma,\gamma} \left(c^\dagger_{j\sigma\gamma} c_{i\sigma\gamma} + \text{H.c.}\right) + \sum_{j,\gamma,\sigma} \Delta_\gamma n_{j\sigma\gamma}, \quad (1)$$

where $c^\dagger_{j\sigma\gamma}$ creates an electron at the chain site j, with spin z-axis projection σ, and on orbital γ (either orbital a or orbital b). $t_{\rm hop}$ is the hopping integral. For simplicity, we considered only intraorbital hoppings along the chain, and we used identical hopping for both orbitals [$t_a = t_b = t_{\rm hop} = 1$]. Δ_γ denotes the crystal-field term, and $n_{j\sigma\gamma}$ is the orbital-resolved number operator at site j. We fix the crystal-field parameters as $\Delta_a = 4.1$ and $\Delta_b = 0$. The large crystal field $\Delta_a = 4.1 \gtrsim 4t_{\rm hop}$ ensures that only orbital b is occupied in the noninteracting ground state because the bandwidth W of orbital a is $W = 4t_{\rm hop}$ [Fig. 1(a)].

The electronic interaction portion is canonical:

$$H_{\rm in} = U \sum_{j,\gamma} n_{j\uparrow\gamma} n_{j\downarrow\gamma} + \left(U' - \frac{J_H}{2}\right) \sum_{j,\gamma<\gamma'} n_{j\gamma} n_{j\gamma'} - 2J_H \sum_{j,\gamma<\gamma'} \mathbf{S}_{j\gamma} \cdot \mathbf{S}_{j\gamma'} + J_H \sum_{j,\gamma<\gamma'} (P^\dagger_{j\gamma} P_{j\gamma'} + \text{H.c.}). \quad (2)$$

The first term is the on-site Hubbard repulsion between $\uparrow$ and $\downarrow$ electrons in the same orbital. The second term is the electronic repulsion between electrons at different orbitals. The standard relation $U' = U - 2J_H$ arises from the rotational invariance SU(2) symmetry of the Hamiltonian. The third term is the ferromagnetic Hund's interaction between electrons occupying the active two orbitals $\gamma = a, b$ of the same site. $\mathbf{S}_{j\gamma}$ is the total spin of orbital γ at site j. The last term is the pair hopping between different orbitals, where $P_{j\gamma} = c_{j\downarrow\gamma} c_{j\uparrow\gamma}$.

To obtain the ground state $|\Psi_0\rangle$ of this model, we employed the static DMRG method. For our numerical calculations, we use a system size $L = 36$ with two orbitals at each site, and we kept $m = 1200$ states. The exciton Gaussian wave packet is created with spin $\uparrow$ and a crystal momentum k_0, by applying the operator

$$h^\dagger_\uparrow(k_0) = A \sum_j e^{-(j-j_0)^2/2\omega_r^2} e^{-ik_0 j} c^\dagger_{j\uparrow a} c_{j\uparrow b} \quad (3)$$

to the ground state $|\Psi_0\rangle$. This operator excites an electron from the half-filled orbital b to the empty orbital a [Fig. 1(b)], centered at site $j_0 = 18$ and with width $\omega_r = 2.54$. The number 2.54 implies that the size of the initial Gaussian is exactly six lattice spacings at half height, a size that we considered adequate for easy visualization. A is the normalization constant of the Gaussian wave packet. Due to the finite width $\omega_k = 1/2\pi\omega_r$ of the Gaussian wave packet in momentum space, we fix the crystal momentum at $k_0 = -0.5\pi + 4\omega_k$ (i.e., close to the highest occupied electronic level with width $\omega_k = 0.06$). Because we construct a wave packet with a net nonzero momentum [$\mathbf{k_0}(\text{exciton}) = \mathbf{k_e}(\text{electron}) + \mathbf{k_h}(\text{hole})$ at time $t = 0$] that points in our case towards the left, the resulting time evolution will *not* be left-right symmetric.

We investigate numerically the time evolution of the one-exciton state $|\Psi_e\rangle = h^\dagger_\uparrow(k_0)|\Psi_0\rangle$ under the influence of H, i.e., $|\Psi(t)\rangle = e^{-iHt}|\Psi_e\rangle$. To perform the time evolution, we have implemented the Krylov-space decomposition in the DMRG code [28,29]. For the DMRG calculations, at least 1200 states were kept during the time evolution.

To study the dynamics of the excitonic wave packet, we measure the following observables at each time step:

$$\langle n_{ja}(t)\rangle = \langle\Psi(t)|n_{ja\uparrow} + n_{ja\downarrow}|\Psi(t)\rangle, \quad (4)$$

$$\langle n_{jb}(t)\rangle = \langle\Psi(t)|n_{jb\uparrow} + n_{jb\downarrow}|\Psi(t)\rangle, \quad (5)$$

$$\langle S^z_{ja}(t)\rangle = \langle\Psi(t)|(n_{ja\uparrow} - n_{ja\downarrow})/2|\Psi(t)\rangle, \quad (6)$$

$$\langle S^z_{jb}(t)\rangle = \langle\Psi(t)|(n_{jb\uparrow} - n_{jb\downarrow})/2|\Psi(t)\rangle, \quad (7)$$

$$\langle \tau_{zj}(t)\rangle = \langle\Psi(t)|n_{ja} - n_{jb}|\Psi(t)\rangle, \quad (8)$$

where $\langle n_{ja}(t)\rangle$ and $\langle n_{jb}(t)\rangle$ are the orbital-resolved time-dependent charge densities of orbitals a and b. $\langle S^z_{ja}(t)\rangle$ and $\langle S^z_{jb}(t)\rangle$ are the respective orbital-resolved z components of the time-dependent spin densities. $\langle \tau_{zj}(t)\rangle$ is the z component of the time-dependent orbital density. All these quantities are site dependent.

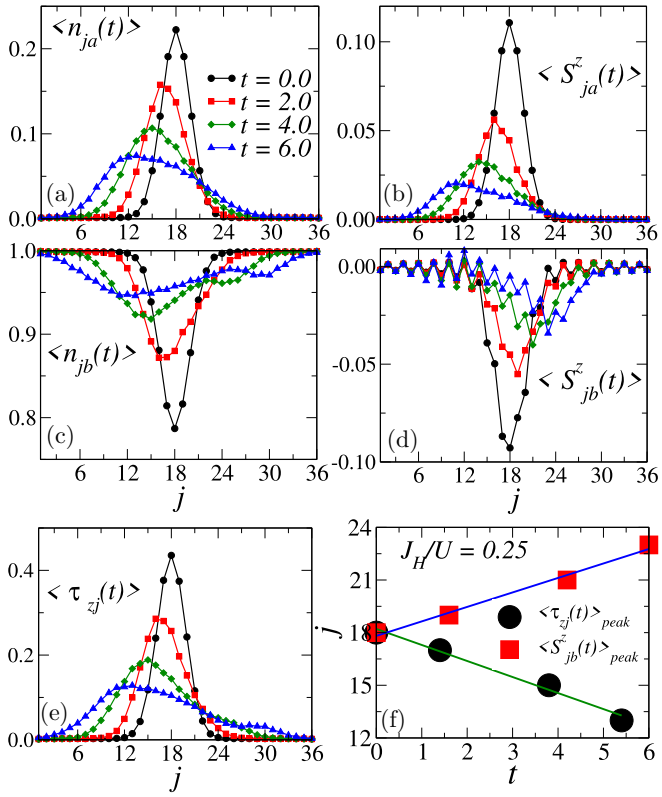

FIG. 2. Snapshots of the evolution of wave packets at different times: (a) charge density $\langle n_{ja}(t)\rangle$, (b) spin density $\langle S^z_{ja}(t)\rangle$, (c) charge density $\langle n_{jb}(t)\rangle$, (d) spin density $\langle S^z_{jb}(t)\rangle$, and (e) orbital density $\langle \tau_{zj}(t)\rangle$. At $t = 0$, wave packets are at the center of the system, i.e., site $j_0 = 18$. (f) Positions of the peaks of the orbital (black circles) and spin (red squares) wave packets vs t. The peak positions are fitted with straight lines to extract the velocity of orbital and spin wave packets. These results were obtain at $J_H/U = 0.25$ and $U/W = 1.0$ using t-DMRG for a system with $L = 36$ sites.

(a) Dynamics of an exciton in a two-orbital model. The Hamiltonian ground state, at overall quarter filling ($L = 36$ and total number of electrons $N_e = 36$) and parameters $U/W = 1.0$, $J_H/U = 0.25$ [30], and $\Delta_a = 4.1$, results in a situation where orbital b is a half-filled Mott insulator with AFM-spin correlations, while orbital a remains empty. At time $t = 0$, the process previously described leads to an exciton centered in the middle of the chain [see Fig. 1(b)], i.e., at site $j_0 = 18$. This results in a hole wave packet $\langle n_{jb}(t)\rangle$ in orbital b [Fig. 2(c)] and an electron wave packet $\langle n_{ja}(t)\rangle$ in orbital a [Fig. 2(a)]. The excitation of an electron from orbital b at $t = 0$ also creates spin excitations $\langle S^z_{ja}(t)\rangle$ with up spins in orbital a [Fig. 2(b)] and down spins in orbital b $\langle S^z_{jb}(t)\rangle$ [Fig. 2(d)].

As shown in Figs. 2(a) and 2(b), with increasing time the charge wave packet $\langle n_{ja}(t)\rangle$ and the spin wave packet $\langle S^z_{ja}(t)\rangle$ at orbital a (the originally empty orbital) move with similar speeds toward the left from the central site $j_0 = 18$, indicating no spin-charge separation for orbital a, as expected for an electron moving in an empty medium. On the other hand, in the half-filled orbital b, the charge wave packet $\langle n_{jb}(t)\rangle$ and spin wave packet $\langle S^z_{jb}(t)\rangle$ move in opposite directions with time, providing clear evidence of spin-charge separation [see Figs. 2(c) and 2(d)] (as expected in interacting one-orbital systems). Interestingly, the charge wave packets $\langle n_{ja}(t)\rangle$ and $\langle n_{jb}(t)\rangle$ move together, as mirror images of each other [see Figs. 2(a) and 2(c)]. The bound state of an electron and hole pair minimizes the on-site interorbital interaction U' [31]. Intuitively, when the hole of orbital b and the electron in orbital a are in the same site, the strong interorbital repulsion energy U' is *not active* (as compared with the case where an electron in orbital a and an electron in orbital b are on the same site resulting in strong interorbital interaction U'). This results in the formation of an electron-hole bound pair exciton which moves as a single entity with increasing time t towards the left of site $j_0 = 18$ [32].

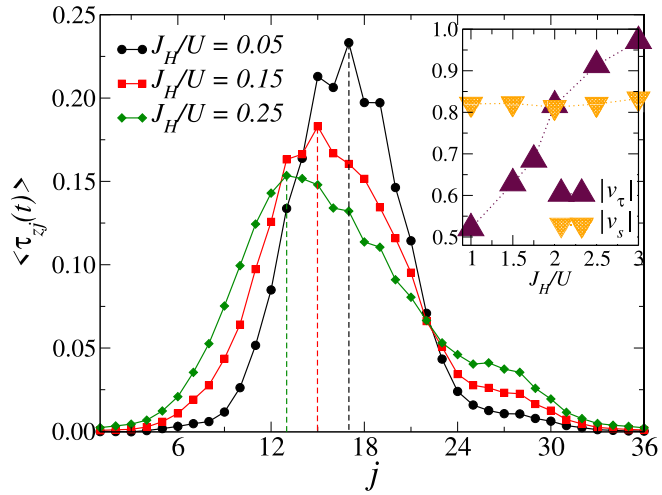

FIG. 3. Orbital density $\langle \tau_{zj}(t)\rangle$ at time $t = 5$ for three values of Hund's interactions J_H/U and at fixed $U/W = 1.0$. Inset: Orbiton and spinon speeds $|v_\tau|$ and $|v_s|$ are parametric with Hund's interaction J_H/U at $U/W = 1.0$.

In the electron-hole pair exciton, the electron promoted from the half-filled orbital b to the unoccupied orbital a is also equivalent to creating an *orbiton* [22,33] because $\langle n_{ja}(t)\rangle$ and $\langle n_{jb}(t)\rangle$ move together as a bound state. Namely, when we use the expression "orbiton" it implies that a bound-state electron-hole pair exists. In Fig. 2(e), we show the orbiton dynamics via $\langle \tau_{zj}(t)\rangle$ evolving with time t. The orbital wave packet $\langle \tau_{zj}(t)\rangle$ moves similarly to $\langle n_{jb}(t)\rangle$ and $\langle n_{ja}(t)\rangle$, towards the left from the central site $j_0 = 18$, while the spin wave packet $\langle S^z_{jb}(t)\rangle$ moves toward the right. Thus our result can be reinterpreted as a signature of spin-orbit separation in real space with increasing time t. To determine the velocities of the orbital and spin excitations, we monitored the positions of the peak values of $\langle \tau_{zj}(t)\rangle$ and $\langle S^z_{jb}(t)\rangle$ versus time. Using simple linear fits to extract the orbiton (v_τ) and spinon (v_s) velocities [Fig. 2(f)], we find that the orbital wave packet ($v_\tau = -0.91$) has a speed only slightly faster than the spin wave packet ($v_s = 0.82$), at $J_H/U = 0.25$ and $U/W = 1.0$.

Next, to study the role of the interorbital repulsion U' and Hund's coupling J_H in the dynamics of the exciton wave packet, we calculate $\langle \tau_{zj}(t)\rangle$ and $\langle S^z_{jb}(t)\rangle$ for different values of J_H/U (but only in the physical region $0 < J_H/U < 1/3$, where U' is not smaller than J_H [30]). Figure 3 displays the orbital wave packet at time $t = 5$ but for three different values

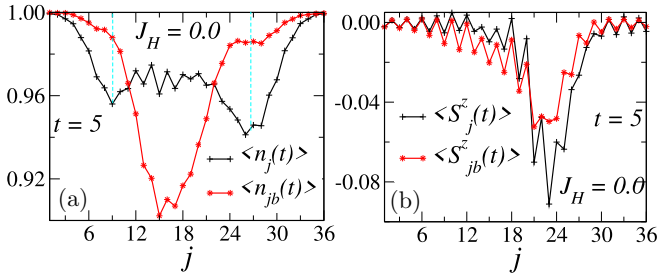

FIG. 4. Comparison of dynamics of a hole in the one-orbital (half filled) and two-orbital (quarter filled) 1D chain at $t = 5$. (a) Charge densities $\langle n_j(t)\rangle$ (one orbital) and $\langle n_{jb}(t)\rangle$ (two orbital). (b) Spin densities $\langle S^z_j(t)\rangle$ (one orbital) and $\langle S^z_{jb}(t)\rangle$ (two orbital).

of J_H/U. We find that for the smaller coupling $J_H/U = 0.05$ the wave packet $\langle \tau_{zj}(t)\rangle$ traveled only a very short distance from the central site $j_0 = 18$. However, increasing the Hund's coupling to $J_H/U = 0.25$, still at time $t = 5$, $\langle \tau_{zj}(t)\rangle$ traveled a larger distance (five lattice spacings) from the central site $j_0 = 18$. The inset shows the orbiton and spinon speeds $|v_\tau|$ and $|v_s|$, respectively, versus J_H/U. We find that the orbital velocity increases significantly with increasing J_H/U, which is in qualitative agreement with Refs. [22,23]. We believe this is because increasing J_H/U reduces the interorbital interaction U', which results in a less-tightly-bound electron-hole pair and thus the exciton becoming less heavy and being able to move at a faster rate $|v_\tau|$. On the other hand, at small J_H/U the interorbital interaction U' increases and results in heavier excitons, which naturally are more localized [7,31]. The larger value of orbiton velocity was observed in RIXS experiments because of the large Hund's coupling in Ca_2CuO_3 [23]. The increase in orbiton velocity was explained in terms of the superexchange process [22,23], where the authors showed that the energy of the intermediate state during the movement of the orbiton depends on the Hund's coupling J_H. For completeness, note that we find that the spin speed $|v_s|$ (inset of Fig. 3) does not change much with increasing J_H/U and remains unaffected by the concomitant modifications in U', which is intuitively reasonable.

(b) Comparison of dynamics of a single hole in one- and two-orbital Hubbard models. In Figs. 4(a) and 4(b), we show a comparison of the dynamics of a hole in the one-orbital Hubbard model (half-filled chain, $U/W = 1.0$) and in the two-orbital Hubbard model (quarter-filled chain, $U/W = 1.0$, $U'/W = 1.0$, and $J_H/U = 0$) chain systems. At $t = 0$, a hole was created at the central site $j_0 = 18$, either by removing an electron at site $j_0 = 18$ for the one-orbital case or, for two orbitals, by removing an electron in orbital b and exciting this electron to orbital a at the same site, $j_0 = 18$. The results for the charge wave packets are remarkably different. While the charge wave packet in the one-orbital system moves quite fast and splits into left- and right-moving wave packets, the charge wave packet in the two-orbital system moves very slowly due to the formation of the strong bound state of electron (in orbital a) and hole (in orbital b). The heaviness of the bound-state electron-hole pair is natural because propagating to the next site involves two hoppings t_a and t_b and an intermediate state with energy proportional to U (scaling as

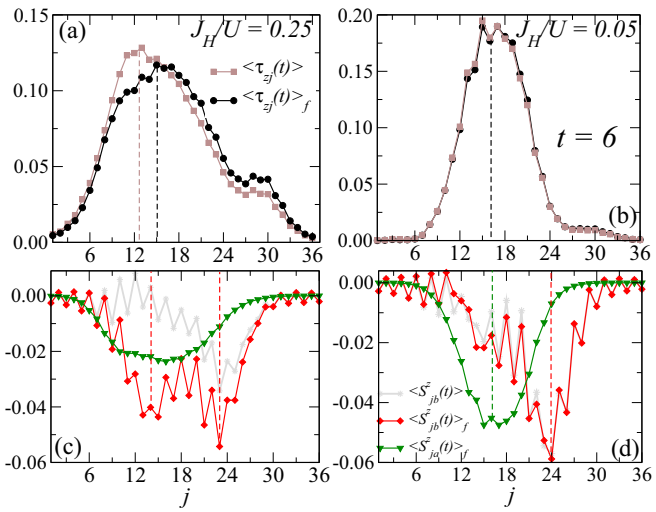

FIG. 5. Comparison of the dynamics of an exciton with and without the spin-flip process. The orbital wave packet with spin flip (without spin flip) $\langle \tau_{zj}(t)\rangle_f$ ($\langle \tau_{zj}(t)\rangle$) is denoted by circles (squares) for (a) $J_H/U = 0.25$ and (b) $J_H/U = 0.05$. Spin wave packets $\langle S^z_{jb}(t)\rangle_f$ (diamonds), $\langle S^z_{ja}(t)\rangle_f$ with the spin-flip process (downward pointing triangles), and $\langle S^z_{jb}(t)\rangle$ without spin flip (stars) for (c) $J_H/U = 0.25$ and (d) $J_H/U = 0.05$. These results were obtained at time $t = 6$ and for $U/W = 1.0$.

$t_a t_b/U$), while the bare hole in one orbital propagates easily with just a hopping $t_{\rm hop}$. Interestingly, the spin wave packets in both systems move with a similar speed and towards the right from the central site $j_0 = 18$ [see Fig. 4(b)]. This is expected because after the separation of spin and charge wave packets in the two-orbital system (at quarter filling), the spin moves approximately guided by the scale $t^2_{\rm hop}/U$, the same scale that the spinon follows in the one-orbital half-filled system [14].

(c) Dynamics of a spin-flipped exciton in a two-orbital model. In the RIXS experiment, during the creation of orbital excitations, spin-flip processes are also allowed [22,23]. Figure 5 presents a comparison of orbiton dynamics with and without spin flip during the exciton generation, for different values of J_H/U. At $t = 0$, for the spin-flip process the exciton wave packet was created by the operator $A\sum_j e^{-(j-j_0)^2/2\omega_r^2} e^{-ik_0 j} c^\dagger_{j\downarrow a} c_{j\uparrow b}$ acting on the ground-state wave function $|\Psi_0\rangle$. We found that the orbital velocity of $\langle \tau_{zj}(t)\rangle_f$ when spin flip occurs is only slightly reduced compared with the previously described non-spin-flip case $\langle \tau_{zj}(t)\rangle$ at $J_H/U = 0.25$ [see Fig. 5(a)]. The slower speed of the spin-flip orbiton compared with the non-spin-flip orbiton, for the multiorbital Hubbard Hamiltonian, is *in contrast to the result-sexpected* from the superexchange picture [23], which predicts a faster speed of the spin-flip orbiton (the movement of the spin-flip orbiton is regulated by $t_a t_b/(U - 3J_H)$, and that of the non-spin-flip orbiton is regulated by $t_a t_b/(U - 2J_H)$) [34]. The slower speed of the spin-flip orbiton [Fig. 5(a)] is presumably due to an attractive interaction between spinon and orbiton in the presence of a large Hund's coupling, as argued in Ref. [22], compared with the without-spin-flip case (where spinon and orbiton repel each other [22]). For a smaller $J_H/U = 0.05$, the results are almost identical, and the orbital wave packet moves very slowly in both cases [see Fig. 5(b)].

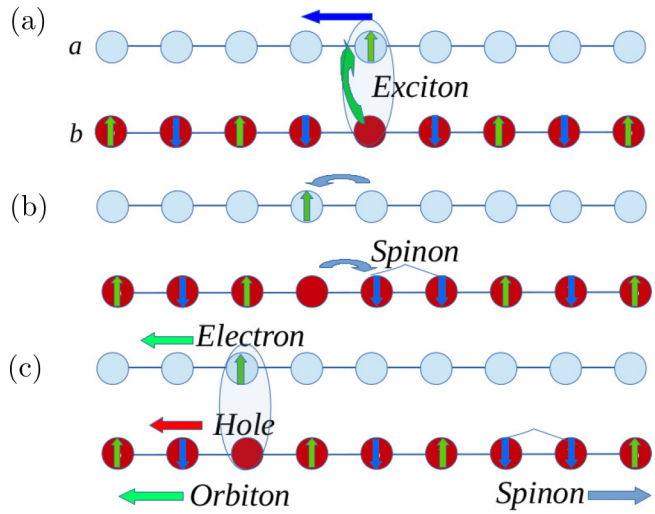

FIG. 6. Illustration of spin-orbit and spin-charge separation in a two-orbital (a and b) one-dimensional chain. (a) An exciton with a finite momentum (blue arrow) is created at $t = 0$ by exciting an electron from orbital b. (b) The electron in orbital a hops towards the left, while an electron with down spin on orbital b hops towards the right (i.e., the hole moves to the left), creating a spinon on orbital b. (c) Electron and hole (orbiton) move in a bound state to the left, while the spinon moves free to the right.

The spin-flip excitonic process leads to the creation of spin wave packets $\langle S^z_{jb}(t)\rangle_f$ and $\langle S^z_{ja}(t)\rangle_f$ in the spin-down state [Fig. 5(c)]. Interestingly, at large J_H/U the spin-wave packet splits into two wave packets with time ($t \gtrsim 3$), traveling in opposite directions (starting at the central site $j_0 = 18$). This curious splitting of the spin wave packet $\langle S^z_{jb}(t)\rangle_f$ indicates the presence of two fractionalized spinons [35]. The left-moving wave packet $\langle S^z_{jb}(t)\rangle_f$ travels with speed similar to that of $\langle S^z_{ja}(t)\rangle_f$ of orbital a and $\langle \tau_{zj}(t)\rangle_f$. This could be due to the strong Hund's interaction between spin wave packets of orbitals a and b, which favors parallel alignment (spin-down state) of spin wave packets $\langle S^z_{jb}(t)\rangle_f$ and $\langle S^z_{ja}(t)\rangle_f$. At large J_H/U, the creation of additional spinons was suggested in the spin-orbital spectrum [22]. The right-moving spin wave packet $\langle S^z_{jb}(t)\rangle_f$ moves with speed similar to that of $\langle S^z_{jb}(t)\rangle$ (without-spin-flip case) [Fig. 5(c)]. On the other hand, for smaller J_H/U, the spin wave packet $\langle S^z_{jb}(t)\rangle_f$ does not split into two parts. $\langle S^z_{jb}(t)\rangle_f$ (spin-flip case) and $\langle S^z_{jb}(t)\rangle$ (without spin flip) move with similar speeds [see Fig. 5(d)].

Conclusions. Using the Krylov-space t-DMRG method, we studied the real-time dynamics of an excitonic wave packet evolving via a two-orbital Hubbard model on a chain, at intermediate coupling U/W. We observed the real-space spin-orbit and spin-charge separation by monitoring the dynamics of spin, charge, and orbital wave packets. We find that the charge and spin wave packets of the higher-energy orbital a move together, whereas the charge and spin wave packets of the lower-energy orbital b move in opposite directions (Fig. 6). The electron in the higher-energy orbital and hole in the lower-energy orbital always move together. The interorbital interactions (U' and J_H) play a crucial role in orbiton dynamics. For example, the orbiton velocity increases significantly by increasing J_H/U, whereas the spinon velocity remains unchanged. Interestingly, we found that *a hole in a one-orbital chain moves much faster than a hole in a two-orbital chain*, because the hole in the lower-energy orbital forms a (heavy) bound pair with the electron in the higher-energy orbital. Moreover, we presented the dynamics of the spin-flipped exciton, where we found evidence of fractional spinons at large Hund's coupling. In future work, our calculations can be extended in various directions that our group, and other groups, has experience with. For example, these calculations can be extended into chain multiorbital systems with spin block states [36,37], electronic models that realize the Haldane $S = 1$ chain and turn superconducting with doping [38], systems with spirals made of spin blocks [39], flux states [40], systems with spin-orbit coupling [41], ladder materials with orbital selective Mott phases [42], systems with intertwined orders [43], materials with orbital order [44], ruthenates [45], and generic t-J models [46]. In all these different contexts, how wave packets will move is not obvious, and surprises may arise.

Acknowledgments. We thank N. Kaushal and N. D. Patel for discussions. B.P. and E.D. were supported by the U.S. Department of Energy (DOE), Office of Science, Basic Energy Sciences (BES), Materials Sciences and Engineering Division. G.A. was partially supported by the Center for Nanophase Materials Sciences, which is a U.S. DOE Office of Science User Facility, and by the Scientific Discovery through Advanced Computing (SciDAC) program funded by the U.S. DOE, Office of Science, Advanced Scientific Computing Research and Basic Energy Sciences, Division of Materials Sciences and Engineering. Validation and some computer runs were conducted at the Center for Nanophase Materials Sciences, which is a DOE Office of Science User Facility.

[1] C. Kim, A. Y. Matsuura, Z.-X. Shen, N. Motoyama, H. Eisaki, S. Uchida, T. Tohyama, and S. Maekawa, Phys. Rev. Lett. **77**, 4054 (1996).
[2] Y. Tokura and N. Nagaosa, Science **288**, 462 (2000).
[3] B. J. Kim, H. Koh, E. Rotenberg, S.-J. Oh, H. Eisaki, N. Motoyama, S. Uchida, T. Tohyama, S. Maekawa, Z.-X. Shen, and C. Kim, Nat. Phys. **2**, 397 (2006).
[4] Y. Matiks, P. Horsch, R. K. Kremer, B. Keimer, and A. V. Boris, Phys. Rev. Lett. **103**, 187401 (2009).
[5] F. C. Zhang and K. K. Ng, Phys. Rev. B **58**, 13520 (1998).
[6] J. Rincón, E. Dagotto, and A. E. Feiguin, Phys. Rev. B **97**, 235104 (2018).
[7] E. Collart, A. Shukla, J.-P. Rueff, P. Leininger, H. Ishii, I. Jarrige, Y. Q. Cai, S.-W. Cheong, and G. Dhalenne, Phys. Rev. Lett. **96**, 157004 (2006).
[8] J. Kim, D. Casa, M. H. Upton, T. Gog, Y.-J. Kim, J. F. Mitchell, M. van Veenendaal, M. Daghofer, J. van den Brink, G. Khaliullin, and B. J. Kim, Phys. Rev. Lett. **108**, 177003 (2012).
[9] J. Kim, M. Daghofer, A. H. Said, T. Gog, J. van den Brink, G. Khaliullin, and B. J. Kim, Nat. Commun. **5**, 4453 (2014).

[10] T. Giamarchi, *Quantum Physics in One Dimension* (Clarendon, Oxford, 2004).

[11] F. D. M. Haldane, J. Phys. C: Solid State Phys. **14**, 2585 (1981).

[12] B. Pandey, E. Dagotto, and S. K. Pati, Phys. Rev. B **102**, 214302 (2020).

[13] J. Voit, Phys. Rev. B **47**, 6740 (1993).

[14] E. A. Jagla, K. Hallberg, and C. A. Balseiro, Phys. Rev. B **47**, 5849 (1993).

[15] K. A. Al-Hassanieh, J. Rincón, E. Dagotto, and G. Alvarez, Phys. Rev. B **88**, 045107 (2013).

[16] O. M. Auslaender, H. Steinberg, A. Yacoby, Y. Tserkovnyak, B. I. Halperin, K. W. Baldwin, L. N. Pfeiffer, and K. W. West, Science **308**, 88 (2005).

[17] C. Kollath, U. Schollwöck, and W. Zwerger, Phys. Rev. Lett. **95**, 176401 (2005).

[18] B. Kumar, Phys. Rev. B **87**, 195105 (2013).

[19] J. Schlappa, K. Wohlfeld, K. J. Zhou, M. Mourigal, M. W. Haverkort, V. N. Strocov, L. Hozoi, C. Monney, S. Nishimoto, S. Singh, A. Revcolevschi, J.-S. Caux, L. Patthey, H. M. Rønnow, J. van den Brink, and T. Schmitt, Nature (London) **485**, 82 (2012).

[20] V. Bisogni, K. Wohlfeld, S. Nishimoto, C. Monney, J. Trinckauf, K. Zhou, R. Kraus, K. Koepernik, C. Sekar, V. Strocov, B. Büchner, T. Schmitt, J. van den Brink, and J. Geck, Phys. Rev. Lett. **114**, 096402 (2015).

[21] K. Wohlfeld, M. Daghofer, S. Nishimoto, G. Khaliullin, and J. van den Brink, Phys. Rev. Lett. **107**, 147201 (2011).

[22] J. Heverhagen and M. Daghofer, Phys. Rev. B **98**, 085120 (2018).

[23] R. Fumagalli, J. Heverhagen, D. Betto, R. Arpaia, M. Rossi, D. Di Castro, N. B. Brookes, M. Moretti Sala, M. Daghofer, L. Braicovich, K. Wohlfeld, and G. Ghiringhelli, Phys. Rev. B **101**, 205117 (2020).

[24] B. Kumar, Phys. Rev. B **79**, 155121 (2009).

[25] S. R. White and A. E. Feiguin, Phys. Rev. Lett. **93**, 076401 (2004).

[26] A. E. Feiguin and S. R. White, Phys. Rev. B **72**, 020404(R) (2005).

[27] Q. Luo, A. Nicholson, J. Rincón, S. Liang, J. Riera, G. Alvarez, L. Wang, W. Ku, G. D. Samolyuk, A. Moreo, and E. Dagotto, Phys. Rev. B **87**, 024404 (2013).

[28] G. Alvarez, L. G. G. V. Dias da Silva, E. Ponce, and E. Dagotto, Phys. Rev. E **84**, 056706 (2011).

[29] G. Alvarez, Comput. Phys. Commun. **180**, 1572 (2009).

[30] This robust Hund's coupling is commonly used in the context of iron-based superconductors; see Q. Luo, G. Martins, D.-X. Yao, M. Daghofer, R. Yu, A. Moreo, and E. Dagotto, Phys. Rev. B **82**, 104508 (2010), and references therein.

[31] C. Yang and A. E. Feiguin, Phys. Rev. B **98**, 035128 (2018).

[32] See Supplemental Material at http://link.aps.org/supplemental/10.1103/PhysRevB.104.L220302 for the dynamics of wave packets at smaller values of the Hubbard coupling.

[33] C. Lane and J.-X. Zhu, Phys. Rev. B **101**, 155135 (2020).

[34] These differences highlight the importance of studying a Hubbard model because the intermediate- and strong-coupling regimes do not necessarily behave equally.

[35] C.-C. Chen, M. van Veenendaal, T. P. Devereaux, and K. Wohlfeld, Phys. Rev. B **91**, 165102 (2015).

[36] B. Pandey, L.-F. Lin, R. Soni, N. Kaushal, J. Herbrych, G. Alvarez, and E. Dagotto, Phys. Rev. B **102**, 035149 (2020).

[37] J. Herbrych, J. Heverhagen, N. D. Patel, G. Alvarez, M. Daghofer, A. Moreo, and E. Dagotto, Phys. Rev. Lett. **123**, 027203 (2019).

[38] N. D. Patel, N. Kaushal, A. Nocera, G. Alvarez, and E. Dagotto, npj Quantum Mater. **5**, 27 (2020).

[39] J. Herbrych, J. Heverhagen, G. Alvarez, M. Daghofer, A. Moreo, and E. Dagotto, Proc. Natl. Acad. Sci. USA **117**, 16226 (2020).

[40] M. Sroda, E. Dagotto, and J. Herbrych, Phys. Rev. B **104**, 045128 (2021).

[41] N. Kaushal, A. Nocera, G. Alvarez, A. Moreo, and E. Dagotto, Phys. Rev. B **99**, 155115 (2019).

[42] N. D. Patel, A. Nocera, G. Alvarez, A. Moreo, S. Johnston, and E. Dagotto, Commun. Phys. **2**, 64 (2019).

[43] B. Pandey, R. Soni, L.-F. Lin, G. Alvarez, and E. Dagotto, Phys. Rev. B **103**, 214513 (2021).

[44] L.-F. Lin, N. Kaushal, Y. Zhang, A. Moreo, and E. Dagotto, Phys. Rev. Mater. **5**, 025001 (2021).

[45] T. Hotta and E. Dagotto, Phys. Rev. Lett. **88**, 017201 (2001).

[46] J. Riera, K. Hallberg, and E. Dagotto, Phys. Rev. Lett. **79**, 713 (1997).